

Proposal of self-excited wound-field magnetic-modulated dual-axis motor for hybrid electric vehicle applications

ISSN 1751-8660
Received on 6th May 2017
Revised 18th August 2017
Accepted on 14th September 2017
E-First on 18th December 2017
doi: 10.1049/iet-epa.2017.0285
www.ietdl.org

Masahiro Aoyama¹ ✉, Toshihiko Noguchi², Yuto Motohashi²

¹Electric Component Development Department, SUZUKI Motor Corporation, 300 Takatsuka-cho, Minami-ku, Hamamatsu City, Shizuoka, Japan

²Electrical and Electronics Engineering Department, Shizuoka University, Hamamatsu City, Japan

✉ E-mail: aoyamam@hhq.suzuki.co.jp

Abstract: This study proposes a permanent-magnet (PM)-free magnetic-modulated motor where the magnetic flux variation in a differential frequency between the armature fundamental rotating magnetic field frequency and the rotor rotation speed frequency is effectively utilised for the field magnetisation instead of PMs. The operation principle of the self-excitation with a diode rectifier circuit on the rotor is discussed. Magnetic circuit design and structural design of downsized prototype machine are performed for the purpose of experimental verifications of self-excitation. In addition, the preliminary experimental test results are demonstrated with prototype machine. Consequently, it is confirmed that the proposed PM-free magnetic-modulated motor can automatically obtain the field magnetisation power by utilising differential frequency which is inevitably generated by magnetic-modulation technique.

1 Introduction

A sustainable transportation system can be achieved through the development of high-efficiency vehicles with significantly lower fuel consumption [1]. Recently, the new standards are effectively achievable with electrified powertrains utilising electric motors [2–4]. Electric motors have much higher efficiencies than internal-combustion engines and, thus, require less energy. An interior permanent-magnet (PM) synchronous motor is commonly employed in the most of currently available hybrid and electric vehicles (HEVs, EVs) on the market [5, 6]. With the use of high-magnetic flux density and high-coercivity rare-earth magnets, PM machines can provide high torque density, competing well against other PM-free motor, i.e. an induction machine, and a switched reluctance machine. In addition, differing from battery powered EVs such as Nissan LEAF, HEVs involve two energy sources, e.g. a gasoline and a battery, as well as two powertrain, e.g. an engine and a motor. It is a key challenge that how to effectively combine the engine driving force and the motor driving force with these optimal efficiency driving points.

The typical strong HEVs essentially adopt the same technology, i.e. the planetary-geared electronic-continuously variable transmission system, to combine the engine driving force and the motor driving force. However, this system suffers from the drawbacks of low power density per its unit weight, high transmission loss, abrasion resistant problem, and annoying audible noise. In the case of a compact car which is particularly limited

powertrain mounting space, the lightweight and compact HEV-system means everything. It is because that the ratio of powertrain light weighting contributes to mileage improvement and a drive performance enhancement is bigger than the other class vehicles. To solve such a problem, as shown in Figs. 1a and b, magnetic-modulated dual-axis motor (magnetic-geared dual-axis motor) is proposed for novel HEV-systems [7–24]. By purposely designing the flux-modulating ring of the magnetic gear to be rotatable, it can work as the planetary-gear for the power split HEV system, e.g. Toyota-Hybrid-System-II employed for TOYOTA Prius as shown in Fig. 1c. The engine output power flow can be split into two paths, one path is via the outer rotor (modulator) attached to the transmission (drive shaft) while another path is via the inner rotor (PM rotor) which is connected to the engine output shaft. The traction motor (MG2) and the planetary-gear of the conventional power split HEV system can be integrated into the magnetic-modulated dual-axis motor to form a single machine unit which can realise lightweight and compact HEV system.

On the one side of such the advantages, however, the conventional PM-rotor type magnetic-modulated motor has a serious problem. Rare-earth sintered expensive PMs with a high residual magnetic flux density are selected for a field energy source used in this motor. On the other hand, since rare-earth sintered PMs have a high electric conductivity (not as rare as metals such as copper), eddy current will occur in the PMs, and the risk of demagnetisation will increase with the linkage of asynchronous rotating magnetic flux, which is automatically caused by magnetic-

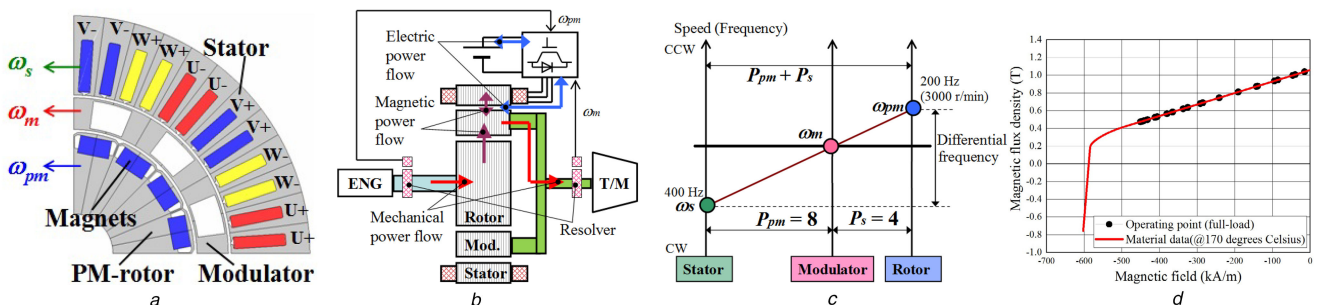


Fig. 1 HEV-system applied magnetic-modulated dual-axis motor (a) Conventional PM-rotor type magnetic-modulated dual-axis motor, (b) HEV-system applied magnetic-modulated dual-axis motor, (c) Collinear chart of magnetic-modulated dual-axis motor, (d) Operating point of magnet permeance under maximum load

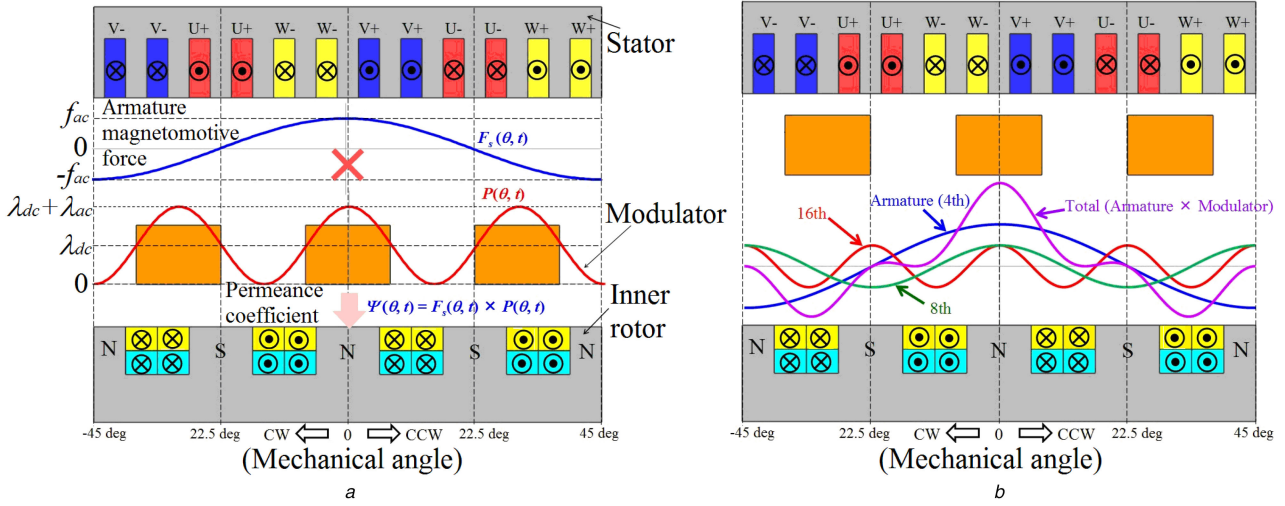


Fig. 2 Modulated magnetomotive force distribution caused by modulator
(a) Armature magnetomotive force and permeance coefficient distribution of modulator, (b) Air-gap magnetic flux waveforms between modulator and inner rotor

modulation principle using pole pieces as shown in Fig. 1d [25–27]. In addition, a high-pole number of PM rotors are available because of synchronisation with the harmonic rotating magnetic field, which is generated by permeance distribution of the modulator. Thus, the large amount of expensive PM is needed. Furthermore, the adjustable speed drive characteristics will be limited in narrow range due to the high induced voltage of PM rotor with the high-pole number.

To solve these problems, a novel PM-free magnetic-modulated dual-axis motor is proposed in this paper. The wound-field rotor (WF rotor) that replace the PMs with electromagnets are consist of self-excited technique applied diode rectifier circuit utilising magnetic flux variation in the differential frequency between the stator rotating magnetic field and the rotor rotation frequency (differential flux). Actually, the self-excited technique is not required that a slip-rings and carbon brushes have to be equipped to inject/withdraw currents into/from the rotating rotor windings. As described in the above, the unique point of the proposed motor can utilise the asynchronous harmonic content (differential flux) which is inevitably generated magnetic flux modulation principle in the asynchronous rotating mode of the armature fundamental frequency and the WF-rotor rotation frequency. In addition, the passive variable magnetic flux function of self-excitation utilising the differential flux has a potential to extend the adjustable speed drive area.

Theoretical analysis of the proposed motor is developed and analytically explained in the discussion that the differential flux can be mainly retrieved for the field magnetisation with the diode rectifier circuit on the rotor. Moreover, its operation performance is analytically investigated through the FE analysis (FEA). Moreover, the self-excitation is experimentally demonstrated through the rotor current measurement via a slip-ring with the downsized prototype. In addition, the torque performance is clarified compared with the benchmark PM-type magnetic-modulated motor.

2 Operation principle

2.1 Magnetic-modulation technique

The magnetic-modulated dual-axis motor is composed of a distributed winding stator and two coaxial rotors, i.e. the outer rotor (modulator) for flux modulation of the armature rotating magnetic field, and the inner rotor which synchronise with the harmonic rotating magnetic field generated by the modulator. Fig. 2 illustrates the magnetic flux waveforms which are modulated by the modulator. Here, the armature magnetomotive force $F_s(\theta, \omega_s t)$ can be expressed as

$$F_s(\theta, \omega_s t) = f_{ac} \cos\{P_s(\theta - \omega_s t) + \delta\} \quad (1)$$

where f_{ac} is an amplitude of armature magnetomotive force, P_s is a pole-pair number of stators, θ is a spatial position, ω_s is an angular velocity of stator, δ is a current phase. Here, the armature magnetomotive force is approximately sinusoidal waveform. Then, the spatial permeance coefficient distribution of the modulator $P(\theta, \omega_m t)$ is given by (2) with approximated sinusoidal waveform, similarly

$$P(\theta, \omega_m t) = \lambda_{dc} + \lambda_{ac} \cos(P_m \theta - \gamma) \cos P_m \omega_m t, \quad (2)$$

where λ_{dc} is the constant part, and λ_{ac} is the amplitude of the periodical variations. P_m is a pole number of the modulators, γ is an offset angle and ω_m is an angular velocity of the modulator. Here, the range of the variation is $0 < P(\theta, \omega_m t) < 1.0$. Thus, the magnetic flux in the air gap between the modulator and the rotor, i.e. the magnetic-modulated armature magnetic flux $F_g(\theta, t)$ is obtained by the vector product between (1) and (2)

$$\begin{aligned} F_g(\theta, \omega_s t, \omega_m t) &= F_s(\theta, \omega_s t) P(\theta, \omega_m t) \\ &= f_{ac} \lambda_{dc} \cos\{P_s(\theta - \omega_s t) + \delta\} \\ &\quad + \frac{1}{2} f_{ac} \lambda_{ac} \cos(P_m \theta - \gamma) \\ &\quad \times \left\{ \begin{aligned} &\cos((-P_s \omega_s + P_m \omega_m)t + P_s \theta + \delta) \\ &+ \cos(-(P_s \omega_s + P_m \omega_m)t + P_s \theta + \delta) \end{aligned} \right\} \end{aligned} \quad (3)$$

As expressed in the above expression, the magnetic flux in the air gap is composed of the three different rotating magnetic fields, i.e. the first term is the armature fundamental rotating magnetic field, the second and the third terms correspond to the harmonic rotating magnetic fields of the pole pairs $(P_m - P_s)$ and $(P_m + P_s)$. Then, the rotor angular velocity ω_{pm} must be satisfied the following relations to synchronise in the modulated harmonic rotating magnetic field

$$P_{pm} \omega_{pm} = -(P_s \omega_s \pm P_m \omega_m) \quad (4)$$

where P_{pm} is a pole-pair number of PM rotors. The magnetic permeability of the air-gap reluctance generally decreases with respect to frequency increase so that it is common to apply the following pair:

$$P_m \omega_m - P_{pm} \omega_{pm} = P_s \omega_s \quad (5)$$

Thus, as expressed in (6), rotation speed of the modulator can be variably changed with respect to PM-rotor speed in addition to stator excitation frequency

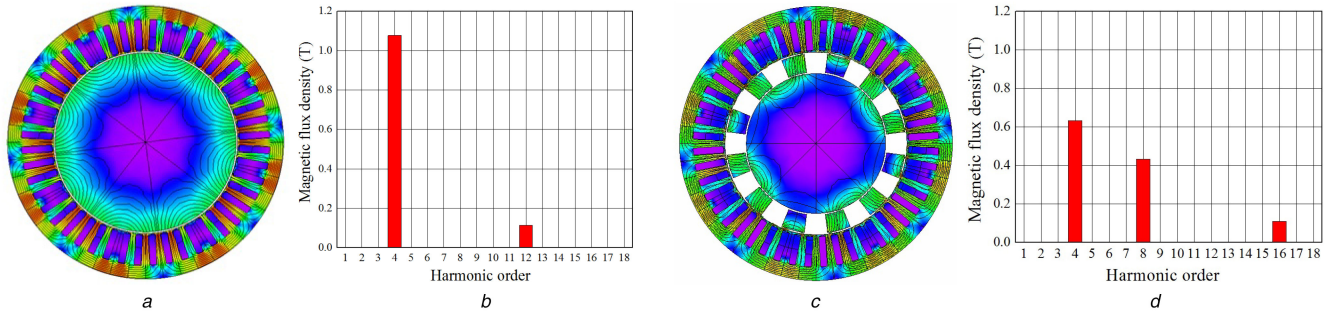


Fig. 3 Magnetic flux density, flux lines, and harmonic contents

(a) Magnetic flux density and flux lines without modulator, (b) Harmonic contents in air gap without modulator (in mechanical angle), (c) Magnetic flux density and flux lines with modulator, (d) Harmonic contents in air gap between inner rotor and modulator with modulator (in mechanical angle)

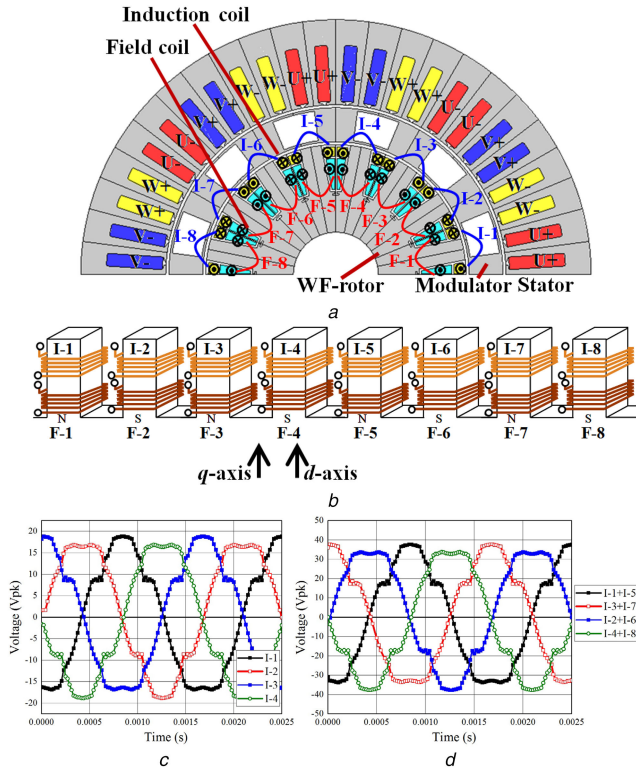


Fig. 4 Proposed PM-free magnetic-modulated dual-axis motor and its induced voltages by differential flux

(a) Proposed PM-free magnetic-modulated dual-axis motor, (b) Inner-rotor windings opened (upper side is induction coils, lower side is field coils), (c) Induced voltages of I-coil (induction-coil), (d) Combination in the same phase of induced voltages

$$\omega_m = \frac{P_{pm}}{P_m} \omega_{pm} + \frac{P_s}{P_m} \omega_s \quad (6)$$

The above expression means that collinearity relation of Fig. 1c is established. In addition, without considering the power losses occurred in the proposed motor, it yields

$$T_s = \frac{P_s}{P_m} T_m + \frac{P_s}{P_{pm}} T_{pm} \quad (7)$$

where T_s is the stator reaction torque, T_m is the modulator torque, T_{pm} is the PM-rotor torque. Since dual-axis drive is possible by applying power split HEV in the automotive applications, collinear chart relation is composed of outer rotor (modulator) attached to the final driveline (drive shaft) and inner rotor connected to the engine shaft for an HEV system with torque reinforcement effect with the magnetic gear.

On the other hand, the first term of (3) indicates that the magnetic flux variation in a differential frequency between the armature rotating magnetic field and the rotor rotation frequency (differential flux) links into the rotor. Therefore, in the case of

conventional PM-rotor type, the eddy current in the PMs will extremely occur due to the large variation of the synchronous magnetic flux, e.g. differential flux. It consequently occurs in operation principle of the magnetic-modulated motor using pole pieces (modulator), which generates the magnetic flux permeance distribution in air gaps. As a result, the operation point of the magnetic flux density in the magnet of typical PM-rotor type extremely changes by an opposing magnetic field with respect to magnet permeance changes as shown in Fig. 1d. In this figure, the red solid line shows the demagnetisation curve at 170°C of Nd-Fe-B ($B_r = 1.22$ T, $H_{cb} = 965.7$ kA/m at 20°C/ $B_r = 1.05$ T, $H_{cb} = 602$ kA/m at 170°C) and black dot shows the operating point of magnetic flux density in the magnet under the opposing magnetic field of the operating condition in Fig. 1c. Because the permeance in the magnet has greatly changed by the differential frequency, it is demanded that a high coercivity magnet is used for the magnetic-modulated motor. Fig. 3 shows the magnetic flux density distribution, flux lines and its harmonic contents of the distributed winding stator and solid inner rotor with or without the modulator (outer rotor) in a 4-pole-pair stator and a 12-pole modulator. As can be seen in this figure, it can be confirmed that the magnetic fluxes of the armature winding in the fundamental frequency (fourth in mechanical angle) are modulated to the eight and the sixteen rotating magnetic flux in mechanical angle by the modulator as indicated in (3).

2.2 Self-excitation technique

To solve the drawback of the conventional PM-type magnetic-modulated motor, a novel self-excited WF magnetic-modulated motor is proposed in this paper as shown in Fig. 4a. The WF rotor that replaces the PMs with electromagnet coil are consist of self-excitation technique applied diode rectifier circuit utilising the differential frequency between the armature magnetic flux rotating field and the rotor rotation speed for field magnetisation power. As expressed in (3), the differential flux can generate induced voltage in rotor coils by Faraday's law. Fig. 4b illustrates the rotor winding with opened where I and F indicate two types of windings, i.e. an induction coil (I-coil) that retrieves mainly the differential flux and a field coil (F-coil) for the field magnetisation. When the proposed PM-free magnetic-modulated motor is operated under the drive condition in Fig. 1c, the induced voltage waveforms of I-coil occurs as shown in Fig. 4c. The induced voltage is mainly caused by the linkage of the differential flux, i.e. the fourth rotating magnetic field in Fig. 3d. Moreover, Fig. 4c indicates only the induced voltage from the I-1 to the I-4 to become the symmetry at the mechanical angle 90° in a period with the pole combinations of $P_s = 4$, $P_m = 12$, $P_{pm} = 8$. For example, I-1, I-5, I-9, and I-13 become the same waveform pattern. On the other hand, the differential flux also links to the rotor coil in orthogonal direction and it is necessary to consider that the induced voltage occurs in all coils wound on salient poles, including the F-coils. As shown in Fig. 4d, every coil is connected in series in a group with the same voltage phase pair for utilising induced voltage in the I-coil, effectively. As shown in Fig. 5a, the I-coil pair of the reverse phase is connected in forward direction and reverse direction to a common cathode to be coil pair which can cancel the induced

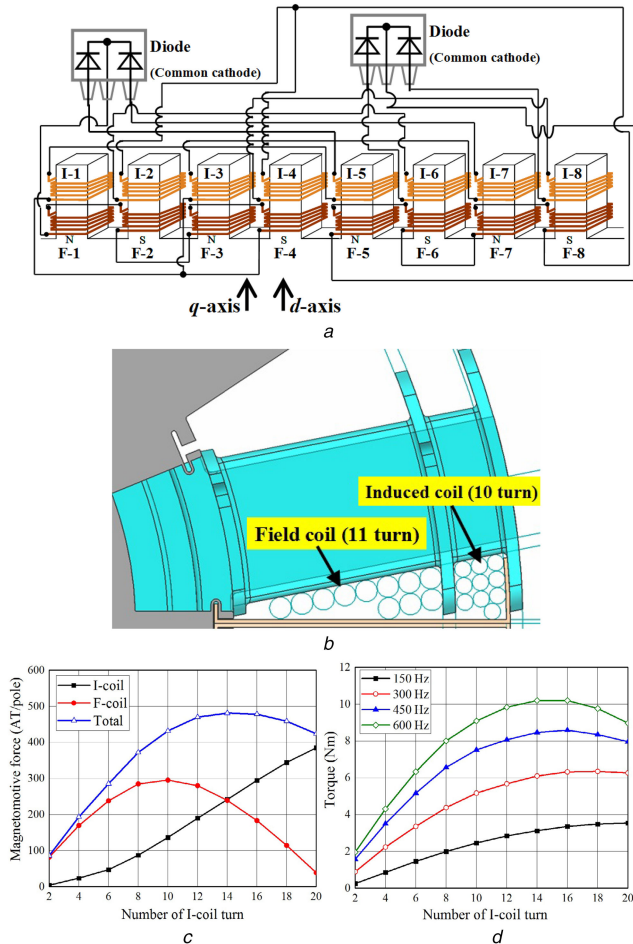


Fig. 5 Wound-field rotor rectifier circuits (four pole-pairs), slot space factor and relationship of number of I-coil turns and magnetomotive force in I-coil and F-coil
 (a) Wound-field rectifier circuits (four pole-pairs), (b) Rotor slot space factor of prototype, (c) Number of I-coil turns-versus-magnetomotive force in I-coil, and F-coil (FEA results), (d) Number of I-coil turns-versus-modulator torque with respect to differential frequency between armature fundamental rotating magnetic field frequency and WF-rotor rotation frequency

voltage in F-coil pair. The magnetic decoupling between I-coil and F-coil can improve the output torque per rotor current ratio and torque ripple reduction. The rotor winding rectifier circuit consists of four series connected coils to reduce rotor copper loss and four segmented diode rectifier circuits. To accomplish this, it is extremely important to select the F-coil pair which the induced voltage can be cancelled. Thus, the F-coil is exclusively used for the field magnetisation pole, i.e. electromagnet pole. The proposed motor is able to utilise inherent dissipated power energy from the differential flux (fourth rotating magnetic field) by applying an electromagnetic induction principle of induction machine and a diode rectifier technique of self-excitation [28].

Next, the rotor magnetomotive force design is explained by regulating coil-turn balance of I-coil and F-coil. Fig. 5b shows the rotor winding space factor in the case of I-coil turn number is 10 and F-coil turn number is 11 as an example. As a result of insulation designs such as insulator bobbin and motor size of prototype machine for operation principle inspection, rotor winding of 21 coil-turns in the sum of I-coil and F-coil per one pole can be wound on inner rotor. Fig. 5c shows the magnetomotive force on each rotor coil with respect to the number of I-coil turns which is simulated in the drive condition in Fig. 1c. As can be seen in Fig. 5c, it can guess that the most suitable ratio for the distribution of I-coil and F-coil exists. Then, the frequency-dependent characteristics of the magnetomotive force balance between the I-coil and F-coil are inspected by FEA. Fig. 5d shows the modulator torque with respect to the number of I-coil and differential frequency of differential flux. As shown in this figure, it can be

confirmed that the maximum torque point has the frequency dependence of magnetomotive force balance between the I-coil and F-coil. Moreover, it can be confirmed that the rotor induced current characteristics changes by the number of the turn ratios between the I-coil, F-coil, and the differential frequency. As for the prototype design, the number of rotor coils is selected as I-coil is 10 turn, F-coil is 11 turn from the limitation of the rotor current density.

3 Downsized prototype machine

Fig. 6a shows the WF-rotor structure and the diode module which is mounted on the rotor coil end cover. Fig. 6b shows the WF rotor where the I-coils and the F-coils are installed to the rotor salient poles. The rotor coils wound via an insulator bobbin, and mechanically reinforced with a resin-mould process to prevent destruction by the centrifugal force under a high speed rotation, and to ensure electric insulation. Figs. 6c and d show the actual WF rotor assembly and benchmark PM-rotor type inner rotor, respectively. Fig. 7a shows the modulator structure with the Poly Phenylene Sulfide resin bar contained in the cavity area between pole piece and this resin bar plays a role in transmitting the torque. Furthermore, each material is adjusted the concentricity by spigot joint portion structure. Figs. 7b and c show the actual modulator assembly, and stator assembly, respectively. The both rotors (the modulator and the WF rotor) can be independently driven, and the positional information of the modulator and the WF rotor can be acquired by using two resolvers as shown in Fig. 7d. And, these rotors are controlled by exciting the angular velocity of the armature current which is calculated by using (6). Specifications of the downsized prototype are listed in Table 1.

4 Preliminary experimental test

4.1 Self-excited rotor current

In the preliminary experimental test, the principle of self-excitation technique utilising differential flux which is inevitably generated by the flux modulation technique as described in Section 2. As shown in Fig. 8, the rotor current in the diode forward and reverse directions for one rectifier circuit is measured via a slip-ring to demonstrate the self-excitation by the differential frequency between the armature fundamental rotating magnetic field frequency and the WF-rotor rotation frequency. Fig. 9a shows the armature current (U-phase) and rotor current waveforms (induced current in forward and reverse directions) under $360 A_{rms}T$ for WF-rotor speed 650 r/min, and its experimental condition is shown in Fig. 9b.

Here, in the preliminary experimental test of rotor current measurement, the output shaft of modulator is mechanically locked. The inverter carrier frequency is set at 10 kHz, and used universal inverter. In this experimental test, the load test of the motor is limited in the low-speed range (under 1000 r/min) and low-armature magnetomotive force (under $450 A_{rms}T$) due to the capitals maximum speed range and mechanical stress of slip-ring. By referring to rotor current waveforms in Fig. 9a, the induced current flows forward and reverse at time intervals. In addition, one period of the induced current accords to the differential frequency. Thus, it can be easily confirmed that the magnetic flux at the differential frequency links to rotor windings and the electromagnet poles can be organised by the field current generated with full-bridge rectifier as shown in Fig. 8d. Fig. 9c shows the induced currents in the forward direction with modulator output shaft locked under $200 A_{rms}T$ for WF rotor 500 and 700 r/min. As can be seen in this figure, it is validated that the induced current increases with respect to WF rotor rotation speed increases in spite of the same armature magnetomotive force, and it is generated by differential frequency. Thus, it was investigated that the induced voltage to the rotor windings by Faraday's law. As a result, induced current increases, and electromagnet torque increases.

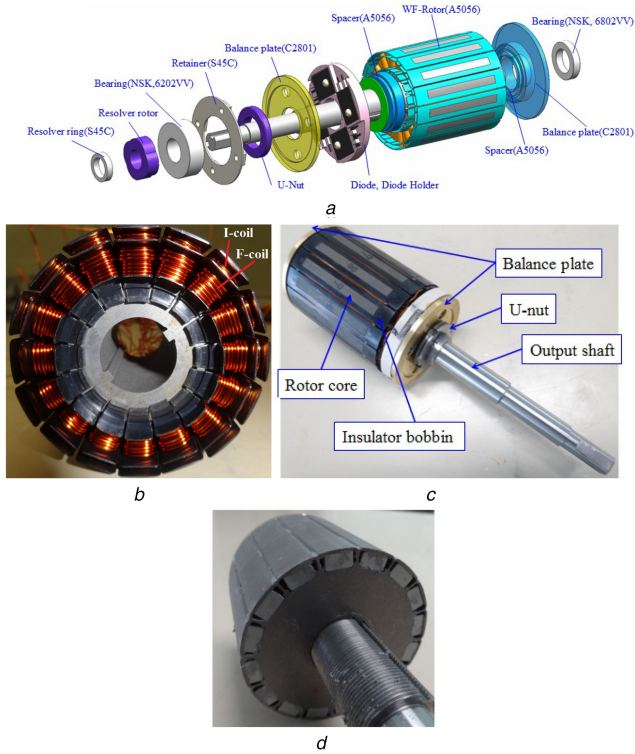


Fig. 6 Actual inner rotor
 (a) Mechanical configuration of WF rotor (inner-rotor), (b) Actual WF rotor with rotor coils, (c) Actual WF rotor assembly, (d) PM-type benchmark inner rotor

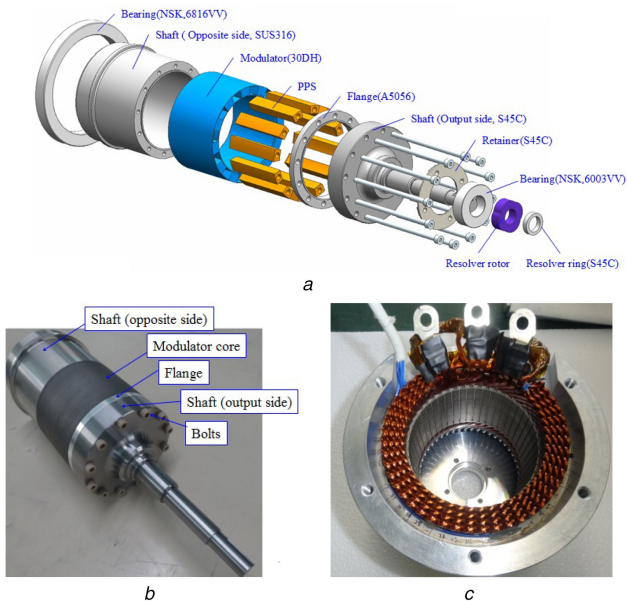


Fig. 7 Actual outer rotor and mechanical configuration
 (a) Mechanical configuration of modulator (outer rotor), (b) Actual modulator assembly, (c) Actual stator assembly, (d) Mechanical configuration

Table 1 Specifications of downsized prototype machine	
number of stator poles	8
number of rotor poles	16
number of modulator poles	12
stator outer diameter	120 mm
rotor diameter	61.2 mm
axial length of core	49.5 mm
air-gap length	0.7 mm
maximum current	150 A _{rms}
armature winding resistance	15.1 mΩ /phase
number of armature coil-turn	8
armature winding connection	4 series–2 parallel
number of I-coil turns	10
number of F-coil turns	11
I-coil resistance	79 mΩ/pole
F-coil resistance	47 mΩ/pole
thickness of iron core steel plate	0.3 mm

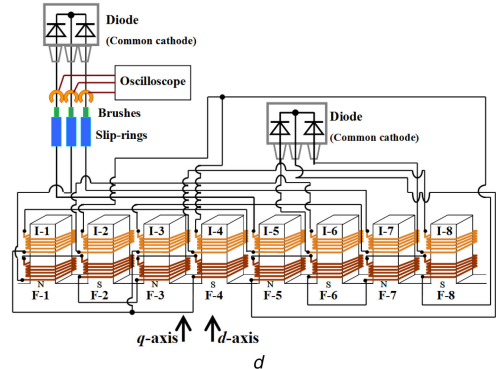
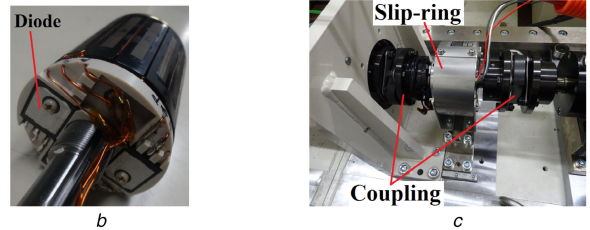
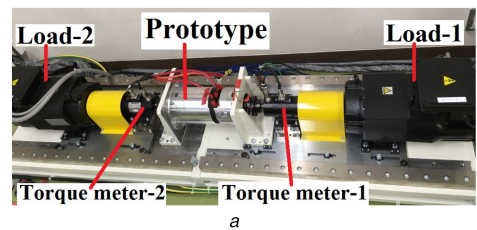


Fig. 8 Experimental setup and rotor current measurement method with slip-ring
 (a) Experimental setup, (b) WF rotor for rotor current measurement, (c) Setup slip-ring, (d) Rotor current measurement method with slip-ring

4.2 HEV simulated driving modes

Fig. 10 illustrates the three driving modes that simulate HEV operations, where collinear charts and simple power flow diagrams are indicated. The following three driving modes are examined through the experiments:

- i an engine assisting mode;
- ii an EV mode; and
- iii a regenerating mode.

The first test is the engine assisting mode, which superimposes the motor output power onto the engine output power, and delivers the synthesised mechanical power to the drive shaft. The second test is conducted under the condition of zero power from the

engine, which is called an EV mode. In the mode, the rotating speed of the inner rotor is fixed at 0 r/min. The last driving mode is the regenerating mode, where some surplus mechanical power

from the engine is regenerated to the inverter through the stator while delivering the mechanical power of the engine to the drive shaft.

The following two points are experimentally checked in each driving mode:

- i relationship between the torque and the gear ratio;
- ii the torque and current phase angle characteristic;

The first focuses on the relationship expressed by (7). As described previously, the two shafts of the proposed motor are connected to the two load machines through the torque meters; it is possible to measure the rotating speed and the torque of the modulator and the inner rotor. The current phase angle β is changed by 15° to check the second point.

The experimental tests were conducted under the inverter conditions of 80 V DC-bus voltage, 10 kHz switching frequency, 4 μ s dead time. The measurement of the torque was performed every 0.5 s to calculate an average value for 15 s of the measured torque. In addition, the drive performances of proposed PM-free dual-axis motor were compared with the PM-type benchmark dual-axis motor, which is shown in Fig. 6d.

Figs. 11a and b show the relationship between the torque and the q -axis current with keeping $i_d = 0$. i_q is varied every 20 A over the range from 10 to 90 A.

In the case of PM-type benchmark, it is confirmed from the figure that the torque of the modulator T_m and the torque of the inner rotor T_{pm} are delivered in proportional to i_q regardless of the driving modes. However, in the case of WF-type proposed motor, T_m and T_{pm} are not delivered in proportional to i_q under all driving modes, but these are approximated by a quadratic function. Furthermore, the torque varies according to the driving mode. This is because, in the case of WF-type proposed motor, as described previously, the field magnetisation power depends on the differential flux amplitude and differential frequency. The differential frequency under the three driving modes of Fig. 10 is 60 Hz (engine assist mode), 100 Hz (EV mode), and 160 Hz (regeneration mode), respectively. In the case of proposed PM-free dual-axis motor, this result means that it is necessary to be driven by the collinearity relations not only with operating the high engine efficiency area but also with keeping the high differential frequency.

On the other hand, as the theoretical equation from (7) indicates, the relationship between T_m and T_{pm} is

$$T_{pm} = -\frac{P_{pm}}{P_m} T_m = -\frac{2}{3} T_m \quad (8)$$

The measured T_m and T_{pm} almost agree with the theoretical values well as the magnetic-gear function.

Next, the torque and the current phase angle characteristics are shown in Figs. 11c and d, respectively, which are measured under

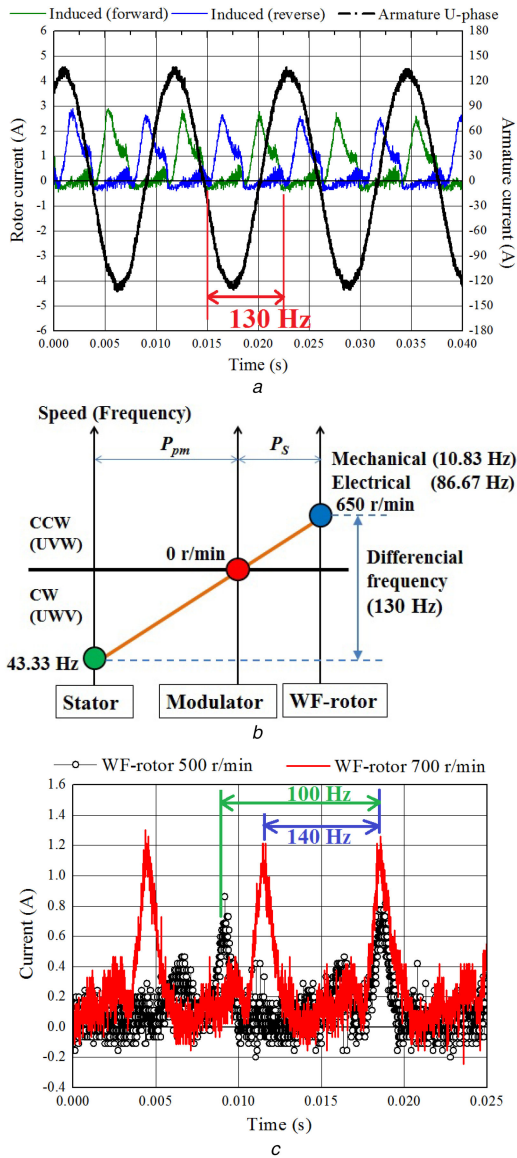


Fig. 9 Collinear chart of experimental test condition and induced currents with respect to WF-rotor rotation speed

(a) Collinear chart of experimental test condition, (b) Induced currents in forward direction with respect to WF-rotor rotation speed, (c) Induced currents in forward direction with respect to WF-rotor rotation speed

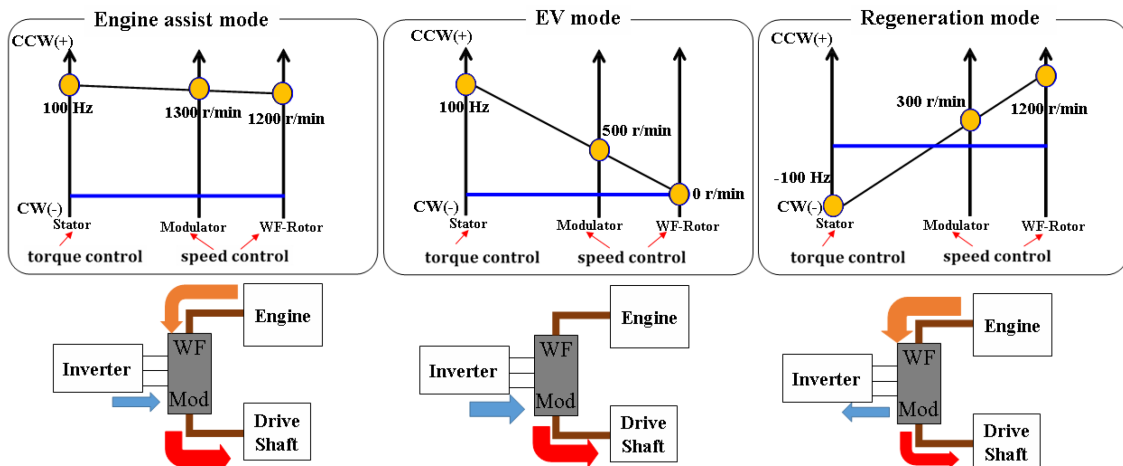


Fig. 10 Driving modes assuming HEV system, collinear charts, and power flow of proposed motor

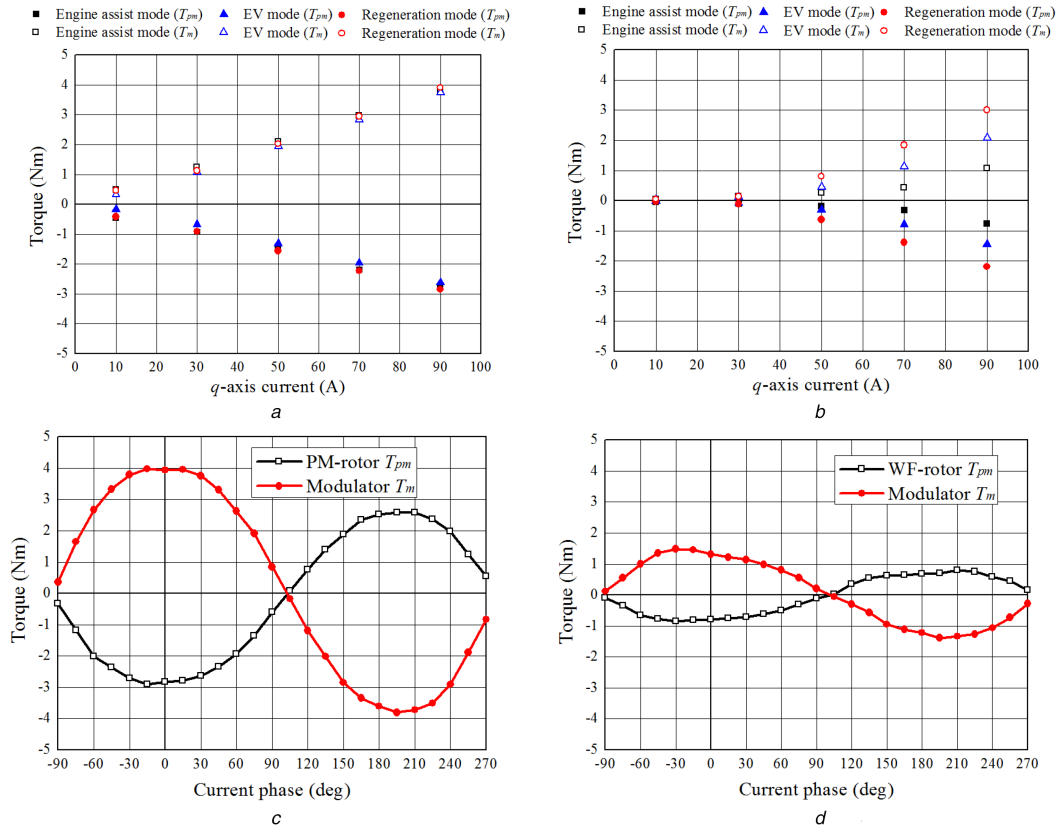


Fig. 11 *q*-axis current versus torque characteristics, and current phase versus torque characteristics (a) *q*-axis current versus torque characteristics of PM-type benchmark, (b) *q*-axis current versus torque characteristics of WF-type proposed, (c) Current phase versus torque characteristics of PM-type benchmark, (d) Current phase versus torque characteristics of WF-type proposed

the condition of the engine assisting mode. The reference phase angle $\beta = 0^\circ$ is defined at the *q*-axis position, and the current phase angle β is varied every 15° from 0° to 360° . The current vector norm is also kept constant at 90 A in the test. Since the PM-type benchmark has near the surface PM structure of the rotor, the similar characteristic to the surface PM synchronous motor is obtained. In the case of WF type proposed PM-free motor, the max torque per ampere point exists in the flux intensifying area. This is because that the reluctance torque can obtain by the saliency ($L_d > L_q$) and the self-excitation technique utilising differential flux generates the electromagnet torque.

5 Conclusion

This paper presented a newly PM-free magnetic-modulated dual-axis motor where the differential frequency between the armature fundamental rotating magnetic field frequency and the WF-rotor rotation frequency is utilised for the field magnetisation instead of PMs. The operating principle has analytically discussed. In addition, the prototype design for operating principle evaluation has been revealed. Furthermore, preliminary experimental test for the verification of self-excitation technique was demonstrated through the rotor current measurement via a slip-ring, and basic torque characteristics. The future work of this study is to demonstrate dual-axis drive, e.g. efficiency maps, range of speed, and torque characteristics of the actual prototype machine in each HEV simulated driving modes through experimental tests. To accomplish this, it is necessary to complete the voltage equation of the magnetic-modulated motor. In addition, the study of optimal dual-axis driving mode with keeping high differential frequency for the torque density increase is important. Furthermore, it is also important to develop the mathematical model to estimate the induced current and the field current of the rotor windings for torque improvement and rotor winding temperature prediction.

6 References

- [1] 'United States Environmental Protection Agency (EPA) accessed on 24 August 2015', <http://www2.epa.gov/science-and-technology/sustainable-practices-science>
- [2] Momoh, O.D., Omoigui, M.O.: 'An overview of hybrid electric vehicle technology'. IEEE Vehicle Power and Propulsion Conf. 2009 (VPPC'09), September 2009, pp. 1286–1292
- [3] Frieske, B., Kloetzke, M., Mauser, F.: 'Trends in vehicle concept and key technology development for hybrid and battery electric vehicles'. 27th Int. Electric Vehicle Symp. and Exhibition 2013 (EVS 27), November 2013, pp. 1–12
- [4] Costa, A.D., Kim, N., Berr, F.L., *et al.*: 'Fuel consumption potential of different plug-in hybrid vehicle architectures in the European and American contexts'. 26th Int. Electric Vehicle Symp. and Exhibition 2012 (EVS 26), Los Angeles, United States, 2012
- [5] Sato, Y., Ishikawa, S., Okubo, T., *et al.*: 'Development of high response motor and inverter system for the Nissan LEAF electric', SAE Technical Paper, 2011, No. 2011-01-0350
- [6] 'Chevrolet HP', <http://www.chevrolet.com/volt-electric-car.html>
- [7] Takeuchi, Y., Kato, H., Tago, M., *et al.*: 'Operating principle and control method of the magnetic modulated motor'. IEEJ Annual Meeting, 2013, No. 5-041, pp. 73–74 (in Japanese)
- [8] Fukuoka, M., Nakamura, K., Kato, H., *et al.*: 'A consideration of the optimum configuration of flux-modulated type dual-axis motor'. IEEJ Technical Meeting, 2013, RM-13-141 (in Japanese)
- [9] Niguchi, N., Hirata, K.: 'A novel magnetic-gear motor', *Jpn. Soc. Appl. Electromagn. Mach.*, 2013, **21**, (2), pp. 110–115 (in Japanese)
- [10] Faus, H.T.: 'Magnet gearing', U.S. Patent 2,243,555, 27 May 1941
- [11] Atallah, K., Calverley, S., Howe, D.: 'Design, analysis and realization of a high-performance magnetic gear', *IEEE Proc. Electr. Power Appl.*, 2004, **151**, (2), pp. 135–143
- [12] Huang, C.C., Tsai, M.C., Dorrell, D.G., *et al.*: 'Development of a magnetic planetary gearbox', *IEEE Trans. Magn.*, 2008, **44**, (3), pp. 403–412
- [13] Montague, R.G., Bingham, C.M., Atallah, K.: 'Magnetic gear dynamics for servo control'. IEEE Proc. the 15th IEEE Mediterranean Electrotechnical Conf. (MELECON2010), 2010, pp. 1192–1197
- [14] Atallah, K., Howe, D.: 'A novel high-performance magnetic gear', *IEEE Trans. Magn.*, 2001, **37**, (4), pp. 2284–2846
- [15] Jian, L., Chau, K.T., Gong, Y., *et al.*: 'Comparison of coaxial magnetic gears with different topologies', *IEEE Trans. Magn.*, 2009, **45**, (10), pp. 4526–4529
- [16] Wang, L.L., Shen, J.X., Wang, Y., *et al.*: 'A novel magnetic-gear outer-rotor permanent-magnet brushless motor'. IEEE Proc. the 4th IET Conf. Power Electronics, Machines and Drives 2008 (PEMD2008), 2008, pp. 33–36
- [17] Wang, L.L., Shen, J.X., Luk, P.C.K., *et al.*: 'Development of a magnetic-gear permanent-magnet brushless motor', *IEEE Trans. Magn.*, 2009, **45**, (10), pp. 4578–4581

- [18] Jian, L., Chau, K.T., Jiang, J.Z.: 'An integrated magnetic-gear permanent-magnet in wheel motor drive for electric vehicles'. IEEE Proc. Vehicle Power and Propulsion Conf. (VPPC), 2008, pp. 1–6
- [19] Jian, L., Chau, K.T.: 'Design and analysis of a magnetic-gear electric-continuously variable transmission system using finite element method', *Prog. Electromagn. Res.*, 2010, **7**, pp. 47–61
- [20] Jian, L., Chau, K.T.: 'Design and analysis of integrated Halbach-magnetic-gear permanent-magnet motor for electric vehicle', *J. Asian Electr. Veh.*, 2009, **7**, pp. 1213–1219
- [21] Wang, J., Atallah, K., Calverley, S.D.: 'A magnetic continuously variable transmission device', *IEEE Trans. Magn.*, 2011, **47**, (10), pp. 2815–2818
- [22] Atallah, K., Wang, J., Calverley, S.D., *et al.*: 'Design and operation of a magnetic continuously variable transmission', *IEEE Trans. Ind. Appl.*, 2012, **48**, (4), pp. 1288–1295
- [23] Black, D.T., Calverley, S.D., Birchall, J.G.: 'The delivery of magnetic powersplit technology'. JSAE Annual Congress, 2016, No. 20165062, pp. 326–333
- [24] Fukuoka, M., Nakamura, K., Kato, H., *et al.*: 'A novel flux-modulated type dual-axis motor for hybrid electric vehicles', *IEEE Trans. Magn.*, 2014, **50**, (11), p. 8202804
- [25] Tonari, T., Kato, H., Matsui, H.: 'Study on iron loss of flux modulated type dual-axis motor'. IEEJ Technical Meeting, 2013, RM-13-142 (in Japanese)
- [26] Fukuoka, M., Nakamura, K., Ichinokura, O.: 'Experimental test and efficiency improvement of surface permanent magnet magnetic gear', *IEEJ J. Ind. Appl.*, 2014, **3**, (1), pp. 62–67
- [27] Husain, M., Hirata, K., Niguchi, N.: 'Design, optimization, and realization of salient-pole electromagnetic gear for variable-transmission applications', *IEEJ J. Ind. Appl.*, 2013, **2**, (1), pp. 87–97
- [28] Nonaka, S.: 'The self-Excited type single-phase synchronous motor', *IEEJ J. Trans. Ind. Appl.*, 1958, **78**, (842), pp. 1430–1438 (in Japanese)